pISSN 1229-3008 eISSN 2287-6251
Progress in Superconductivity and Cryogenics
Vol.23, No.4, (2021), pp.6~9 https://doi.org/10.9714/psac.2021.23.4.006

Effect of capacitive coupling in superconducting coplanar waveguide resonator

Geonwoo Baek, Bongkeon Kim, Sara Arif, and Yong-Joo Doh*

Department of Physics and Photon Science, Gwangju Institute of Science and Technology (GIST), Gwangju 61005, Korea

(Received 24 November 2021; revised or reviewed 15 December 2021; accepted 16 December 2021)

Abstract

Superconducting coplanar waveguide (SCPW) resonators with high quality (Q) factor are widely used for developing quantum sensors and quantum information processors. Here we conducted numerical simulations of SCPW resonators to investigate the relationship between the Q factor and the coupling capacitance of the resonator. Varying the geometrical shape of both ends and coupling parameters of the SCPW resonator resulted in a change of the coupling capacitances and the Q factor as well. Our calculation results indicate that the performance of the SCPW resonator is highly sensitive to the capacitive coupling and searching for an optimal coupling condition would be crucial for developing high-performance SCPW resonator.

Keywords: superconductivity, coplanar waveguide resonator, quality factor, capacitive coupling

1. INTRODUCTION

Superconducting coplanar waveguide (SCPW) resonators, which consist of superconducting resonators capacitively coupled to a microwave transmission line, play a crucial rule in the development of photon detector [1], spin-ensemble sensor [2], superconducting and spin qubits [3]. Moreover, gate-tunable superconducting qubit [4] and topological qubit [5] are studied using the SCPW resonators combined with nano-hybrid Josephson junctions [6] and topological insulators [7]. For developing these superconducting quantum devices, it is crucial to design highly sensitive SCPW resonators.

The sensitivity of the SCPW resonators can be characterized by the quality factor, the so-called Q factor, which is a dimensionless parameter corresponding to the reciprocal of the energy loss within the resonator [8]. The total (loaded) Q factor, Q_l, is given by $1/Q_l = 1/Q_i + 1/Q_c$, where Q_i is the internal Q factor and Q_c is the coupling Q factor. It is known that Q_i is inversely proportional to the microwave energy that is dissipated by impurities in the dielectric substrate or due to quasiparticles in the superconductor, while Q_c is inversely proportional to the microwave energy loss through the capacitive coupling between the central transmission line and the resonator [9].

In this work, we conducted numerical calculations based on the finite element method (FEM) to find Q_l with varying geometrical parameters of SCPW resonators to adjust the coupling strength between the resonator and the central transmission line. For a half-wavelength (λ/2) resonator in Fig. 1a, the coupling capacitance was controlled by varying the overlap length (l_0) and gap distance (w) for the finger- and gap-type couplings, respectively, as shown in Fig. 1b-c. For a quarter-wavelength (λ/4) resonator, the elbow length (l) and the intervening distance (g) between the resonator and the transmission line were varied to adjust the coupling capacitance (see Fig. 3a-c). Our calculation results indicate that the loaded Q factor decreases with increasing the coupling capacitance for both λ/2 and λ/4 SCPW resonators and an input power level of the microwave photons entering the resonator should be also considered for the optimal geometric conditions of the resonator. We believe that our calculation results would provide a practical guide to design and develop highly sensitive SCPW resonators.

* Corresponding author: yjdoh@gist.ac.kr

2. METHOD

We used the RF module in COMSOL's Multiphysics software based on the FEM for calculating the loaded Q factor and the coupling capacitance in this work. The sizes of the substrate and the bounding box, which is a box for applying the boundary conditions, for the λ/2 (λ/4) resonator were 10×3×0.5 (4×4×0.5) and 12×4×3 (5×5×1) mm^3, respectively. The overall length of the λ/2 (λ/4) resonator was fixed to be L = 24 (5.89) mm, corresponding to the fundamental resonance frequency of f_0 = 2.48 (5.02) GHz, which were close to the experimental values obtained from Nb-based SCPW resonators [10]. The theoretical expression of f_0 is given by $f_0 = [2/(1+\varepsilon)]^{1/2}(c/2L)$ for the λ/2 resonator and $[2/(\varepsilon+1)]^{1/2}(c/4L)$ for the λ/4 resonator, where ε means the effective dielectric parameter of the substrate (ε = 11.7 for Si) and c is the speed of an electromagnetic wave in vacuum [11].

The characteristic impedance (Z_0) of the central transmission line and the resonator were matched to 50 Ω for an efficient power transfer and reduced distortion of the signal. We set the width (s) of the central transmission line

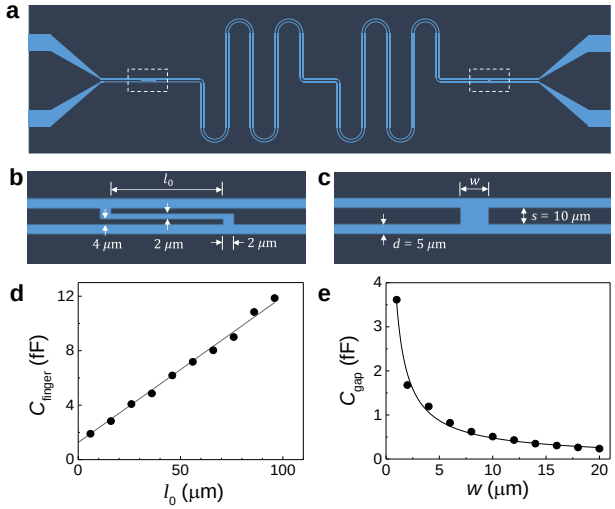

Fig. 1. (a) Schematic of the half-wavelength resonator. Dark (light) blue-colored area means superconducting (insulating) region. White dashed boxes indicate the capacitive couplings. Magnified views of the capacitive couplings of (b) finger-end and (c) gap-end types. (d) Capacitance vs. overlap length for the finger-end type. The solid line is a linear fit to the calculation results (e) Capacitance vs. gap distance for the gap-end type. The solid line is the power-law fit.

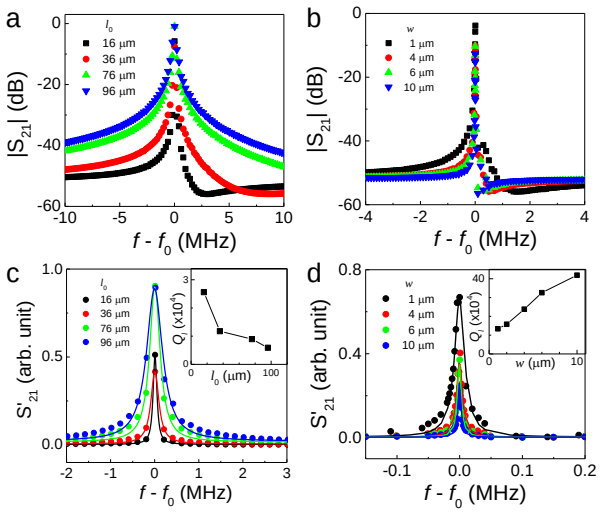

Fig. 2. Microwave transmission spectrum around the resonance frequency for different values of (a) overlap length and (b) gap distance of the half-wavelength resonator. (c) The resonance line shape around the resonance frequency, converted from (a). The solid lines are the Lorentzian fits. Inset: the loaded Q factor for different l0. The line is to guide the eye. (d) The resonance line shape converted from (b). The solid lines are the Lorentzian fits. Inset: the loaded Q factor for different w. The line is to guide the eye.

and the gap distance (d) between the transmission line and the lateral grounded planes to be s = 10 (12) μm and d = 5 (6.5) μm, respectively, for the λ/2 (λ/4) resonator (see Fig. 1c and 3c). Using conformal mapping techniques [12] the geometric capacitance (C_g) and inductance (L_g) per unit length of the resonator were found to be C_g = 171 (166) pF/m and L_g = 414 (424) nH/m for the λ/2 (λ/4) resonator, resulting in $Z_0 = [L_g/C_g]^{1/2}$ = 50 Ω. Here, we assumed that L_g was much larger than the kinetic inductance (L_k). Since L_k is sensitive to the material parameters of the superconducting film used in the experiment [13], the geometric dimensions of s and d should be modified to satisfy the condition of impedance matching.

3. RESULT ANF DISCUSSION

The coupling capacitances ($C_{coupling}$) in the λ/2 resonator are displayed in Fig. 1d-e as a function of the overlap length (l_0) and gap distance (w) for the finger- and gap-type couplings, respectively. It is clearly shown that the finger-type capacitance (C_{finger}) increases linearly with l_0 and the gap-type capacitance (C_{gap}) decreases with w, resulting $C_{gap} \sim w^{-0.9}$. We note that the coupling capacitance was controlled in a range between 0.3 and 12 fF in this work. Progressive changes of the transmission ($|S_{21}|$) spectrum with varying l_0 and w are shown in Fig. 2a and 2b, respectively. We obtained the resonance frequency f_0 = 2.581 ± 0.004 GHz for the λ/2 resonators, which was very close to the theoretical expectation.

The loaded Q factor was obtained by fitting the transmission spectrum to a Lorentzian line. The $|S_{21}|$ transmission spectrum was converted into the linear scale, S'_{21}, using the relation [8] $|S_{21}| = 20 \log_{10}(S'_{21})$, as shown in Fig. 2c-d. After fitting the S'_{21} line shape to a Lorentzian line, Q_l was obtained using $Q_l = f_0/\Delta f$ where Δf means the full width at half maximum of the Lorentzian line. The insets of Fig. 2c-d displays Q_l for different values of l_0 and w. It should be noted that the highest (lowest) value, Q_l = 4.2×10^5 (6.0×10^3), was obtained for the weakest (strongest) coupling capacitance with C_{gap} = 0.51 fF (C_{finger} = 12 fF) in our calculation. When the resonator is overcoupled, it is expected [8] that , $Q_l \sim Q_c \propto C_{coupling}^{-2}$ which is consistent with our calculation results.

The transmission spectra of the λ/4 resonator are displayed in Fig. 4a-b for different values of g and l. We converted the $|S_{21}|$ transmission spectrum into the resonance line shape of S'_{21}, as shown in Fig. 4c-d, and fitted the S'_{21} curve to the hanger equation [14]:

$$S'_{21} = \left|A\left(1+\alpha\frac{f-f_0}{f_0}\right)\left(1-\frac{Q_l/Q_e}{1+2iQ_l(f-f_0)/f_0}\right)\right| \quad (1)$$

where A is the transmission amplitude parameter, α is a linear variation parameter in the overall transmission background around the resonance, and Q_e is a complex-valued Q factor satisfying $\mathrm{Re}[1/Q_e] = 1/Q_c$. The imaginary part of $1/Q_e$ reflects an asymmetry in the resonance line shape. As a result, we obtained Q_l as a function of the intervening distance (g) and the elbow length (l) in Fig. 4e and f, respectively. It is discernible that Q_l decreases in the strong coupling regime with smaller g and longer l, which is similar to the previous results obtained in the λ/2 resonator. We note that Q_l is maximized at g = 30 μm (see Fig. 4e) and at l = 25 μm (Fig. 4f) in the weak coupling regime, suggesting that there exists an optimal geometric condition on the coupling capacitance. The decrease of Q_l

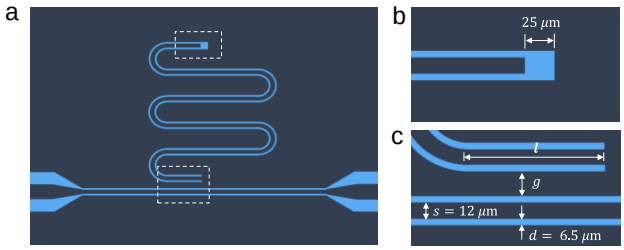

Fig. 3. (a) Schematic of the quarter-wavelength resonator. Dark (light) blue-colored area means superconducting (insulating) region. White dashed boxes indicate the capacitive coupling to the transmission line and its opposite end. Magnified views of (b) the end of the resonator and (c) the capacitive coupling.

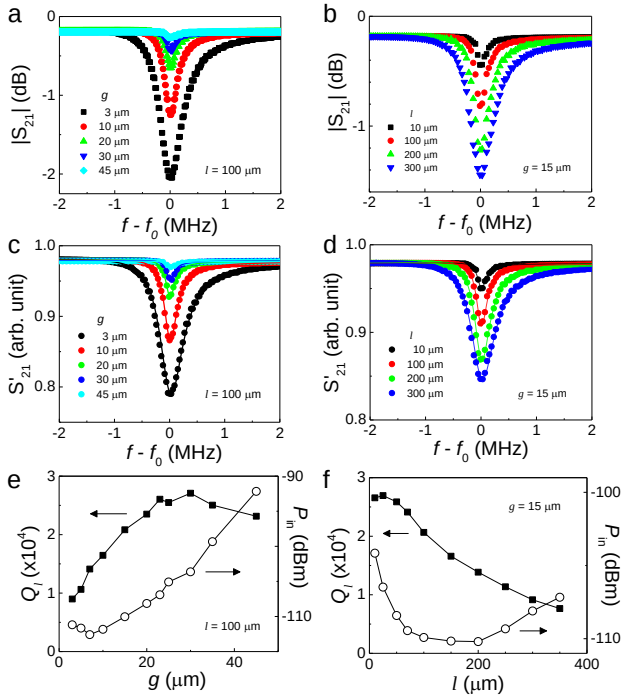

Fig. 4. Microwave transmission spectrum around the resonance frequency for different values of (a) the intervening distance and (b) the elbow length of the quarter-wavelength resonator. (c-d) The resonance line shape around the resonance frequency, converted from (a) and (b), respectively. The solid lines are the hanger fits using Eq. 1. (e) The loaded Q factor and input power as a function of g for l = 100 μm. The lines are used to guide the eye. (f) The loaded Q factor and input power as a function of l for g = 15 μm. The lines are used to guide the eye.

with increasing l is attributed to an increase of the inductive coupling between the feedline and resonator [15].

The input power (P_{in}) at the transmission line provides an additional criterion for the optimal operation of the SCPW resonator. When the input power increases, the resonator is populated with more photons and operates away from the quantum regime. It is known that the average number of photons absorbed in the resonator is given by $\langle n_{ph} \rangle = 2Q_l^2 P_{in}/\hbar\omega_0^2 Q_c$, where $\hbar$ is the reduced Planck's constant and ω_0 is the resonant angular frequency [14]. We plotted P_{in} as a function of the geometric parameters such as g and l in Fig. 4e-f with assuming $\langle n_{ph} \rangle$ = 100. P_{in} becomes a minimum at conditions of g = 7 μm in Fig. 4e and l = 150 μm in Fig. 4f, which deviate from the conditions for the maximum Q_l. Thus it would be necessary to choose an appropriate median values of the geometric dimensions for optimal operation of the SCPW resonator.

4. CONCLUSION

In summary, we conducted numerical calculations of the SCPW resonators to obtain the Q factor, which is dependent on the coupling capacitance between the resonator and the transmission line. The Q_l factor of the half-wavelength resonator increased monotonously with decreasing the coupling capacitance, favoring the gap-end type instead of the finger-end one. The quarter-wavelength resonator, however, exhibited a maximum Q_l value at optimal conditions of the geometric dimensions of the capacitive coupling. The P_{in} for the operation of the resonator was obtained using the quality factors as a function of the geometric parameters. Our calculation results indicate that the performance of the SCPW resonator is highly sensitive to the capacitive coupling and searching for the high-Q_l and low-P_{in} condition would be crucial for developing high performance SCPW resonator.

ACKNOWLEDGMENT

This study was supported by the NRF of Korea through the research program (2018R1A3B1052827 and 2019M3E4A80146) and the GRI grant funded by GIST in 2021.

REFERENCES

[1] P. K. Day, H. G. LeDuc, B. A. Mazin, A. Vayonakis, and J. Zmuidzinas, "A broadband superconducting detector suitable for use in large arrays", Nature 425, pp. 817-821, 2003.

[2] Y. Kubo, F. R. Ong, P. Bertet, D. Vion, V. Jacques, D. Zheng, A. Dréau, J. F. Roch, A. Auffeves, F. Jelezko, J. Wrachtrup, M. F. Barthe, P. Bergonzo, and D. Esteve, "Strong Coupling of a Spin Ensemble to a Superconducting Resonator", Physical Review Letters 105, pp. 140502, 2010.

[3] A. Wallraff, D. I. Schuster, A. Blais, L. Frunzio, R. S. Huang, J. Majer, S. Kumar, S. M. Girvin, and R. J. Schoelkopf, "Strong coupling of a single photon to a superconducting qubit using circuit quantum electrodynamics", Nature 431, pp. 162-167, 2004; K. D. Petersson, L. W. McFaul, M. D. Schroer, M. Jung, J. M. Taylor, A. A. Houck, and J. R. Petta, "Circuit quantum electrodynamics with a spin qubit", Nature 490, pp. 380-383, 2012.

[4] G. de Lange, B. van Heck, A. Bruno, D. J van Woerkom, A. Geresdi, S. R Plissard, E. P A M Bakkers, A. R Akhmerov, and L. DiCarlo, "Realization of Microwave Quantum Circuits Using Hybrid Superconducting-Semiconducting Nanowire Josephson Elements", Physical Review Letters 115, pp. 127002, 2015.

[5] E. Ginossar and E. Grosfeld, "Microwave transitions as a signature of coherent parity mixing effects in the Majorana-transmon qubit", Nature Communications 5, pp. 4772, 2014.

[6] Y.-J. Doh, J. A. van Dam, A. L. Roest, E. P. A. M. Bakkers, L. P. Kouwenhoven, and S. De Franceschi, "Tunable supercurrent through semiconductor nanowires", Science 309, pp. 272, 2005; B.-K. Kim,

H.-S. Kim, Y. Yang, X. Peng, D. Yu, and Y.-J. Doh, "Strong Superconducting Proximity Effects in PbS Semiconductor Nanowires", ACS Nano 11, pp. 221-226, 2017.

[7] H.-S. Kim, T.-H. Hwang, N.-H. Kim, Y. Hou, D. Yu, H. S. Sim, and Y.-J. Doh, "Adjustable Quantum Interference Oscillations in Sb-Doped Bi_2Se_3 Topological Insulator Nanoribbons", ACS Nano 14, pp. 14118-14125, 2020.

[8] L. Frunzio, A. Wallraff, D. Schuster, J. Majer, and R. Schoelkopf, "Fabrication and characterization of superconducting circuit QED devices for quantum computation", IEEE Transactions on Applied Superconductivity 15, pp. 860-863, 2005.

[9] J. M. Sage, V. Bolkhovsky, W. D. Oliver, B. Turek, and P. B. Welander, "Study of loss in superconducting coplanar waveguide resonators", J. Appl. Phys. 109, pp. 063915, 2011.

[10] B. Kim, M. Jung, J. Kim, J. Suh, and Y.-J. Doh, "Fabrication and characterization of superconducting coplanar waveguide resonators", Progress in Superconductivity and Cryogenics 22, pp. 10-13, 2020.

[11] M. Göppl, A. Fragner, M. Baur, R. Bianchetti, S. Filipp, J. M. Fink, P. J. Leek, G. Puebla, L. Steffen, and A. Wallraff, "Coplanar waveguide resonators for circuit quantum electrodynamics", J. Appl. Phys. 104, pp. 113904, 2008.

[12] R.N. Simons, *Coplanar waveguide circuits, components, and systems.* (John Wiley & Sons, 2004).

[13] K. Watanabe, K. Yoshida, T. Aoki, and S. Kohjiro, "Kinetic Inductance of Superconducting Coplanar Waveguides", Japanese Journal of Applied Physics 33, pp. 5708-5712, 1994.

[14] A. Bruno, G. de Lange, S. Asaad, K. L. van der Enden, N. K. Langford, and L. DiCarlo, "Reducing intrinsic loss in superconducting resonators by surface treatment and deep etching of silicon substrates", Appl. Phys. Lett. 106, pp. 182601, 2015.

[15] R. E. George, J. Senior, O.-P. Saira, J. P. Pekola, S. E. de Graaf, T. Lindström, Yu A. Pashkin, “Multiplexing superconducting qubit circuit for single microwave photon generation”, J. Low Temp. Phys. 189, pp. 60, 2017.